OPTICAL PROPERTIES OF NANOCLUSTERS FROM TIME-DEPENDENT DENSITY-FUNCTIONAL THEORY

Laura Koponen

Aalto University School of Science and Technology
Faculty of Information and Natural Sciences
Department of Applied Physics
Espoo, Finland

Dissertation for the degree of Doctor of Science in Technology to be presented with due permission of the Faculty of Information and Natural Sciences for public examination and debate in Auditorium K at Aalto University School of Science and Technology (Espoo, Finland) on the 7th of May, 2010, at 13 o'clock.

Aalto University School of Science and Technology
Department of Applied Physics
P.O.Box 11100
FI-00076 AALTO, Finland

Dissertations of Department of Applied Physics
Aalto University School of Science and Technology
Faculty of Information and Natural Sciences
ISSN 1797-9595 (print)
ISSN 1797-9609 (online)
Dissertation 161 (2010):
Laura Koponen: *Optical properties of nanoclusters from time-dependent density-functional theory*

Opponent:
Prof. Henrik Grönbeck, Chalmers University of Technology, Sweden
Pre-examiners:
Prof. Dage Sundholm, University of Helsinki, Finland
Dr. Esa Räsänen, University of Jyväskylä, Finland
Keywords: *time-dependent density-functional theory, photoabsorption, nanocluster, fullerene, silicon nanocrystal*

ISBN 978-952-60-3128-6 (print)
ISBN 978-952-60-3129-3 (online)
URL: http://lib.tkk.fi/Diss/2010/isbn9789526031293/

Picaset Oy
Helsinki 2010

Abstract

The ground state properties of a quantum-mechanical many-electron system can be effectively modeled by its total electron density only, which is the key idea of the density-functional theory (DFT) methods. However, electronic excitations to higher energy states are not adequately described by the standard DFT formalism. To model the optical properties, for example, absorption and emission and response to time-dependent fields such as laser fields, the extension to time-dependent DFT (TDDFT) has become a popular method.

In this Thesis, the TDDFT methods are utilized to calculate the optical properties of various nanostructures including fullerenes and fullerene derivatives, silicon nanocrystals and metal-polymer hybrid structures. The main focus is in the determination of their photoabsorption spectra using a real-space implementation of TDDFT. By these calculations we study how different structural variations and changes in the chemical environment affect the electronic and optical properties of the materials.

For carbon and boron nitride fullerenes, variations in their size, geometry and doping are found to have a clear impact on their photoabsorption spectra. The results strengthen the view that optical absorption can be effectively used in the experimental characterization of such structures, for example in distinguishing between different isomers.

The photoabsorption is observed to be strongly affected by the chemical environment for both silicon nanocrystals and small silver nanoclusters. When silicon nanoclusters are embedded in silica, the size dependence of their absorption edge is found to change due to major changes in the electronic structure. For the silver clusters, the presence of a polymer is found to bring the absorption edge down to the visible range in some of the studied cases. These calculations shed light to the experimental observations of unexpected absorption from such structures in the visible range.

Tiivistelmä

Kvanttimekaanisen monen elektronin systeemin perustilan ominaisuuksia voidaan kuvata kokonaiselektronitiheyden avulla. Tähän ideaan perustuu tiheysfunktionaaliteoria. Sen puitteissa ei voida kuitenkaan riittävän tarkasti mallintaa virityksiä korkeammille energiatiloille. Optisten ominaisuuksien, esimerkiksi absorption ja emission sekä ajasta riippuvien kenttien kuten laserkenttien kuvaamiseen käytetään nykyään suosittua laajennusta ajasta riippuvaksi tiheysfunktionaaliteoriaksi (TDDFT).

Tässä väitöskirjassa käytetään TDDFT-menetelmää erilaisten nanorakenteiden kuten fullereenien, piinanokiteiden sekä hopeaklusteri-polymeeri-hybridirakenteiden optisten ominaisuuksien laskemiseen. Kiinnostuksen kohteena on erityisesti näiden aineiden optisen absorptiospektrin määrittäminen tietokoneohjelmalla, jossa TDDFT:tä sovelletaan paikka-avaruudessa. Tällaisilla laskuilla tutkitaan, miten erilaiset rakennevaihtelut ja kemiallisen ympäristön muutokset vaikuttavat aineiden sähköisiin ja optisiin ominaisuuksiin.

Tämän työn laskujen perusteella muutokset hiili- ja boorinitridifullereenien koossa, geometriassa ja seostuksessa vaikuttavat selvästi niiden optiseen absorptiospektriin. Tulokset antavat tukea sille, että optisen alueen spektroskopiaa voidaan käyttää tällaisten rakenteiden kokeelliseen tunnistamiseen, esimerkiksi eri isomeerien erottamiseen toisistaan.

Optisen absorption on havaittu riippuvan suuresti kemiallisesta ympäristöstä sekä piinanokiteiden että pienten hopeaklustereiden tapauksessa. Kun piinanokiteet ovat piidioksidin ympäröiminä, niiden minimiabsorptioenergian riippuvuus kiteen koosta muuttuu merkittävien elektronirakenteen muutosten seurauksena. Polymeerin läsnäolon vaikutuksesta hopeaklustereiden minimiabsorptioenergia laskee jossain tutkituista tapauksista näkyvän valon alueelle asti. Nämä tulokset selittävät osaltaan kokeellisia havaintoja kyseisten rakenteiden poikkeuksellisesta näkyvän valon alueen absorptiosta.

Preface

This Thesis has been prepared during the years 2006–2010 in the Academy of Finland Center of Excellence in Computational Nanoscience (COMP) of the Laboratory of Physics. The laboratory is a part of the Department of Applied Physics (previously Department of Engineering Physics and Mathematics) in the Aalto University School of Science and Technology (former Helsinki University of Technology). I have enjoyed the peaceful and relaxed atmosphere in the lab. The local flexible but productive way of working has suited me very well.

Academy professor Risto Nieminen has been the supervisor of my thesis work. He has always done his best to support his graduate students despite all his other duties. The instructor of this work has been professor Martti Puska, our group leader. He has been of great help in preparing the manuscripts. We have also worked hard together to run the Materials Physics courses for the undergraduate students.

At the beginning of my thesis work, always-cheerful Dr. Jan-Ole Joswig was there to help me. I am grateful to my colleague Lasse Tunturivuori for compiling all the codes and having good company throughout the years. During the last year, we had a nice and fruitful collaboration with Dr. Yvette Hancock. Besides my colleagues in the lab, the girls having "Wednesday" lunch are acknowledged for keeping me company at work. Finally, a big hug to my family!

Helsinki, April 2010

Laura Koponen

List of publications

This Thesis consists of an overview and the following publications:

I L. Koponen, M. J. Puska, and R. M. Nieminen, *Photoabsorption spectra of small fullerenes and Si-heterofullerenes*, Journal of Chemical Physics **128**, 154307 (2008) (7 pages). Copyright 2008, American Institute of Physics. Reprinted with permission.

II L. Koponen, L. O. Tunturivuori, M. J. Puska, and R. M. Nieminen, *Photoabsorption spectra of boron nitride fullerenelike structures*, Journal of Chemical Physics **126**, 214306 (2007) (4 pages). Copyright 2007, American Institute of Physics. Reprinted with permission.

III L. Koponen, L. O. Tunturivuori, and R. M. Nieminen, *Effect of the surrounding oxide layer on the photoabsorption spectra of Si nanocrystals*, Physical Review B **79**, 235332 (2009) (6 pages). Copyright 2009, American Physical Society. Reprinted with permission.

IV L. Koponen, L. O. Tunturivuori, M. J. Puska, and Y. Hancock, *Tunability of the optical absorption in small silver cluster–polymer hybrid systems*, arxiv:1003.2183v2 [cond-mat.mtrl.sci]. Accepted for publication in the Journal of Chemical Physics.

The author Laura Koponen has had an active role in all the phases of the research reported in this Thesis. She has been involved in the planning of the simulations and interpreting the results in all the publications. The author performed all the presented calculations and wrote the main drafts of all the publications. The work reported in Publication IV is based on her original idea.

Contents

Abstract iii
Abstract in Finnish iv
Preface v
List of publications vi
Contents vii

1 Introduction **1**

2 Interaction of light with nanostructures **3**
2.1 Electromagnetic response 3
2.2 Ground-state properties of atomic clusters 5

3 Density-functional theory **7**
3.1 Kohn-Sham equations 7
3.2 Exchange and correlation functionals 9
3.3 Pseudopotentials and basis sets 10

4 Time-dependent density-functional theory **11**
4.1 Extension of DFT to the time regime 12
4.2 Linear-response formalism 14
4.3 Computational considerations 16

5 Materials and results **18**
5.1 Fullerenes 18
5.1.1 Small fullerenes 18
5.1.2 Silicon-doped fullerenes 19

5.1.3 Boron nitride fullerenes 21
5.2 Silicon nanocrystals 23
5.3 Silver clusters and their hybrid systems 24

6 Conclusions **30**

Bibliography **32**

Chapter 1

Introduction

In recent decades, the advances in materials and nanostructure fabrication methods have enabled rapid progress towards real nanotechnology and even beyond. Simultaneously, the capabilities of computational science have improved from reliable modeling of a few atoms to systems of hundreds or even thousands of atoms. This is due to the increase in computational power and the development of efficient theoretical and computational methods and techniques.

As the length and time scales of these two approaches come close to each other, new possibilities in nanotechnology appear. Not only more accurate ways of probing and modeling materials become available, but also the possibility of designing and tailoring materials to suit specific needs opens up. In this area, the interplay between computational and experimental research to both directions is emphasized.

The behaviour of nanoscale systems is governed by the laws of quantum mechanics rather than classical mechanics. The electronic and structural properties of matter are determined by the electron wave functions. However, the computational complexity of such systems is very high. An N electron system has namely $3N$ degrees of freedom (three spatial degrees of freedom for each electron) and thus the quantum-mechanical wave function spans a huge Hilbert space. Luckily, a many-electron system can be effectively modeled by its total electron density only, reducing the number of degrees of freedom to three spatial coordinates for the whole system. This is the idea behind the flourishing field of the density-functional theory (DFT) methods [1] founded in the 1960's [2, 3].

However, electronic excitations to higher energy states are not adequately accessible through the standard DFT formalism. Thus many important physical properties remain beyond its scope. These include the electronic phenomena occurring in time, for example, optical properties such as absorption, emission and response to time-dependent fields such as laser fields.

The DFT formalism can be extended to excited states and time-dependent phenomena, resulting in the time-dependent density-functional theory (TDDFT) [4, 5]. The foundations of TDDFT were discovered in the 1980's [6]. During the last decade, a boom both in the applications of TDDFT and in the development of new theoretical methods and their implementation has taken place in the field.

In this Thesis, the TDDFT method is utilized to calculate the optical properties of various nanostructures. The studied materials include fullerenes and fullerene derivatives, silicon nanocrystals and metal-polymer hybrid structures. The main focus is in the determination of their photoabsorption spectra using a real-space implementation of TDDFT. By these calculations we study how different structural variations and changes in the chemical environment affect the electronic and optical properties of the materials.

Chapter 2

Interaction of light with nanostructures

The properties of nanosized materials such as clusters are strongly altered compared with bulk materials and, in addition, totally new phenomena appear. These changes are often due to quantum confinement and other quantum effects. In the interaction with light, continuous scattering and absorption are replaced by resonant interactions when the size of the structure decreases to the scale where each atom counts. In this case, the photon energy needs to match the energy difference of the discrete energy levels of the quantum system. In atoms, molecules and nanoparticles, these individual resonances or electron-hole excitations are often found at optical frequencies and they merge to collective modes such as surface plasmon resonances when the system size increases.

2.1 Electromagnetic response

We briefly review the basic processes of light-matter interaction that are essential to the theme of this Thesis.

Photoluminescence is the process where a substance first absorbs photons by exciting electrons into higher energy states and then emits photons by de-exciting (see Fig. 2.1). The time scale of the whole process is typically very small, of the order of 10 nanoseconds. The individual absorption or emission events happen in femtosecond time scales.

The simplest photoluminescence process where the absorbed and the emitted photons have the same energy is called resonant radiation. In practice, cases where internal energy transitions occur before the emission of the photon are of greater interest. The most studied process is fluorescence, where part of the

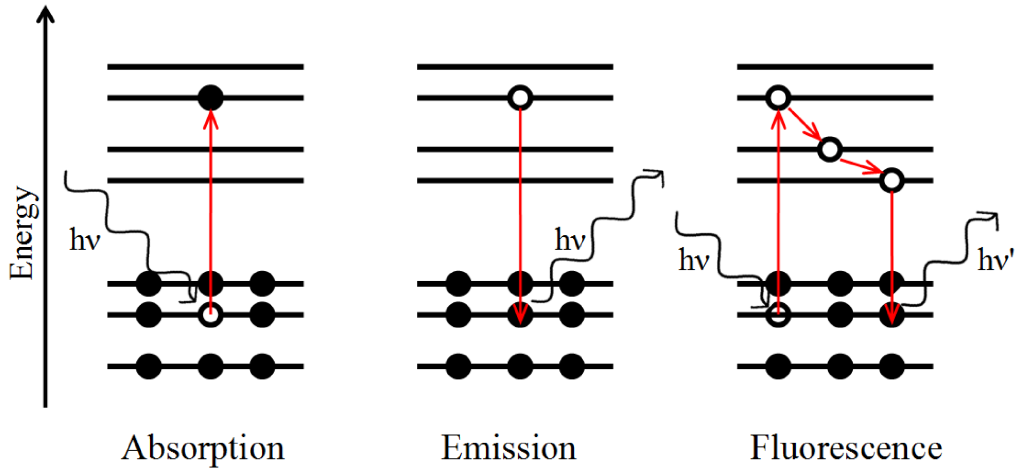

Figure 2.1: Absorption, emission and fluorescence processes described within an energy level diagram.

photon energy is dissipated, leading to emission in lower energy compared with absorption. Another example process that we want to mention is the light amplification by stimulated emission. In this is the emission process, a photon identical to the original one is created in the emission, resulting in a cascade effect in the material.

Optical absorption is a fundamental property of all materials. It determines not only the colour of the material but also many other of its optical properties. Optical absorption is often addressed in computational characterization of matter. This is due to the short time scale and the simplicity of the process, which make it easy to model. Optical absorption is an example of an external perturbation affecting an electron system.

When the more general case of a many-electron system in a time-dependent external field is considered, two cases can be distinguished: the linear and the nonlinear response.

Linear response occurs when certain variables describing the response of matter, such as electronic polarization, are proportional to the variables describing the change in the environment, such as the electric field strength of incoming radiation. In the linear response of molecules and solids, an external field causes a small perturbation in the initial ground state of the system. Within this model, many important physical quantities can be accessed, such as polarizabilities, dielectric functions, excitation energies, photoabsorption spectra and van der Waals coefficients which describe dispersion interactions.

Non-linear response occurs, for example, when matter is in an intense laser field

or when a high-energy projectile such as a proton is scattered by a molecule. In very intense laser fields, some exotic physical phenomena take place. For example, high-harmonic generation occurs when an electron of the atom, molecule or even surface absorbs several photons and then returns to the ground state by absorbing a single photon. This photon has then an integer multiple energy of the driving field. Another example is the above-threshold ionization spectrum. If the intensity of the laser is large enough, the electrons can ionize for any frequency of the applied field through nonlinear processes, not only if the laser frequency is larger than the ionization potential.

Besides the study of the optical properties, the excited-state phenomena play a major role in the research areas of reaction mechanisms and molecular electronics, but they are not addressed in this Thesis. Especially, the *ab initio* molecular dynamics [7] and electron transport [8, 9] are areas where the methodology used in this work – the time-dependent density-functional theory – has great potential.

Different spectroscopies are commonly used in the study of the optical and dielectric properties of materials, including nanomaterials [10]. The most important techniques include electronic absorption of photons (UV-vis), photoluminescence (PL), infrared absorption (IR), Raman scattering, dynamic light scattering and time-resolved techniques, such as transient absorption and time-resolved luminescence. These techniques are based on measuring the absorption, scattering or emission of light.

2.2 Ground-state properties of atomic clusters

We briefly point out a few selected ground-state properties that are related to work reported in this Thesis.

The geometrical atomic structure is the starting point in any description of a cluster or a molecule. However, there is no single experimental technique that could provide direct information on the structure. Clusters and larger molecules are too large for most spectroscopic techniques and too small for diffraction probes. However, a combination of trapped ion electron diffraction [11] together with photoelectron spectroscopy and theoretical *ab initio* calculations [12] can be useful in determining cluster geometries. Studying the reactions with different reagent molecules can be used to gather indirect information (see, e.g., Ref. [13]), but the chance of misinterpretations often remains high. Raman spectroscopy and matrix isolated clusters are recently used in structural determination, but the effect of the matrix on the geometry may not be neglected. Optical spectroscopy can also be used in structure determination, but careful analysis, often including comparisons to theoretical calculations, is needed. Due to all this, competent computational methods are of major importance in determining the cluster and

molecule geometries. The correctness of the calculated geometries must then be verified by comparing the calculated and measured properties of the clusters or molecules.

In the computational structure determination, the minimum energy configurations are searched. Different ground-state properties of candidate structures are usually calculated. In this Thesis, the main ground-state properties of interest are the optimized equilibrium geometries and energy-related quantities, which include ground state energies, energy level structures and energy gaps. They are calculated using the density-functional formalism whose basic theory is presented in Sec. III. Recent advances in computational structure determination include especially global structure optimization techniques (see, e.g., [14]).

Let us make a few brief notes on energy comparisons. When comparing the different structures, total energy differences between the different structures are usually considered instead of absolute energies. The binding energies are often used for clusters that are composed of only one element. The binding energy per atom in a neutral cluster is

$$E_b = -(E_n/n - E_0), \tag{2.1}$$

where n is the number of atoms and E_n the total energy of the cluster, and E_0 is the energy of a free atom. However, the concept of relative stability is often of greater importance in practice. It is measured by the energy gain of adding one atom in the system as

$$\Delta E_n^0 = -\big((E_n - E_{n-1}) - E_0\big), \tag{2.2}$$

The relative stability can be studied in collision or photoinduced fragmentation experiments. The products of the fragmentation process often carry the signatures of the most stable clusters.

Chapter 3

Density-functional theory

In the density-functional theory (DFT) [1], the many-body problem of interacting electrons in an external potential is converted to a simpler problem of non-interacting electrons in an effective potential. As in many other approaches, the nuclei are treated as fixed bodies (the Born-Oppenheimer approximation). Usually, also the relativistic effects are neglected here but can be included in a straightforward way at the scalar-relativistic level. Spin-orbit interactions are then included in a perturbative way.

3.1 Kohn-Sham equations

The static non-relativistic many-electron Schrödinger equation describes the system of N particles as

$$\widehat{H}(\{\boldsymbol{r}_i\})\Psi(\{\boldsymbol{r}_i\}) = E\Psi(\{\boldsymbol{r}_i\}). \tag{3.1}$$

Above, E denotes the total energy of the system and the Hamiltonian consists of terms related to the kinetic energy and to the interactions of electrons with themselves and with an external potential as

$$\widehat{H}(\{\boldsymbol{r}_i\}) = -\frac{1}{2}\sum_{i=1}^{N}\nabla_i^2 + \sum_{i<j}^{N} U(\boldsymbol{r}_i, \boldsymbol{r}_j) + \sum_{i=1}^{N} v_{\text{ext}}(\boldsymbol{r}_i), \tag{3.2}$$

where atomic units ($e = \hbar = m_e = 1$) are used as throughout this Thesis. The external potential usually includes the Coulomb interaction between the electrons and the nuclei. The total particle number N is obtained by an integration of the amplitude of $\Psi(\{\boldsymbol{r}_i\})$ over the whole space.

The exact solution of this equation is a most complex computational task as the wave function of the N electron system, $\Psi(\{\boldsymbol{r}_i\})$, is a function of $3N$ spatial

coordinates. The Hohenberg-Kohn theorem [2] from 1964 states that it is enough to know the ground-state density of the system, $n(\boldsymbol{r})$, to determine all its ground-state properties. More precisely, for a non-degenerate ground state of fermions with a given interaction, $n(\boldsymbol{r})$ uniquely determines the external potential $v_{\text{ext}}(\boldsymbol{r})$ that produced $n(\boldsymbol{r})$. Hence also the Hamiltonian is known. This theorem created the basis for the density-functional theory, whose name comes from the main content of the Hohenberg-Kohn theorem explained above: all the properties of the electron system are *functionals* of $n(\boldsymbol{r})$. Later, the theorem was proven also for degenerate ground states [15].

A practical way of implementing the Hohenberg-Kohn theorem for electronic-structure calculations was presented by Kohn and Sham the very next year 1965 [3]. An auxiliary electron system of non-interacting electrons with exactly the same total electron density is introduced. This fictitious Kohn-Sham system obeys a simple one-particle Schrödinger equation

$$\widehat{H}_{\text{KS}}\psi_j(\boldsymbol{r}) = \varepsilon_j\psi_j(\boldsymbol{r}), \tag{3.3}$$

with the ground state density

$$n_0(\boldsymbol{r}) = \sum_{j=1}^{N} |\psi_j(\boldsymbol{r})|^2, \tag{3.4}$$

where $\psi_j(\boldsymbol{r})$ are the Kohn-Sham orbitals and ε_j the Kohn-Sham eigenvalues. The Kohn-Sham Hamiltonian reads

$$\widehat{H}_{\text{KS}}[n] = -\frac{\nabla^2}{2} + v_{\text{KS}}(\boldsymbol{r}), \tag{3.5}$$

where the effective external potential, namely the Kohn-Sham potential, is usually decomposed as

$$v_{\text{KS}}[n](\boldsymbol{r}) = v_{\text{ext}}[n](\boldsymbol{r}) + v_{\text{H}}[n](\boldsymbol{r}) + v_{\text{xc}}[n](\boldsymbol{r}). \tag{3.6}$$

Above, the first term is the external potential and the second term is the classical electron-electron Hartree interaction. The last term is the exchange-correlation potential which includes all other many-body effects.

The set of equations (3.3)−(3.6) are called the Kohn-Sham equations. Their solution minimizes the total energy functional $E[n] = T_0[n] + E_{\text{ext}}[n] + E_{\text{H}}[n] + E_{\text{xc}}[n]$, where $T_0[n]$, $E_{\text{ext}}[n]$, $E_{\text{H}}[n]$ and $E_{\text{xc}}[n]$ are the kinetic, external potential, Hartree and exchange-correlation terms, respectively. As the exact form of $E_{\text{xc}}[n]$ as well as

$$v_{\text{xc}}[n] = \left.\frac{\delta E_{\text{xc}}[n]}{\delta n}\right|_{n=n(\boldsymbol{r})} \tag{3.7}$$

remain unknown, approximations must be used to evaluate this exchange-correlation term.

3.2 Exchange and correlation functionals

The simplest way to approximate the exchange-correlation functional is the local density approximation (LDA) [3, 16]. Its energy functional is

$$E_{xc}^{\mathrm{LDA}} = \int n(\boldsymbol{r}) \varepsilon_{\mathrm{xc}}^{\mathrm{HOM}}(n(\boldsymbol{r})) d^3r, \tag{3.8}$$

where $\varepsilon_{xc}^{\mathrm{HOM}}(n)$ is the exchange-correlation energy per electron for a homogeneous electron gas with the density n. LDA thus assumes that the exchange-correlation effects at $\boldsymbol{r}$ are fully defined by the local electron density at $\boldsymbol{r}$. All nonlocal dependences are neglected.

Despite its simplicity the LDA functional works surprisingly well for many inhomogeneous electron system even though it does not reach the accuracy required in computational chemistry. For example, LDA typically overbinds giving too short bond lengths. For electron systems with strong spatial variation in the density, the drawbacks are emphasized. In addition, the asymptotic behaviour of the LDA potential far from nuclei is wrong. Therefore, properties such as the ionization potential have large errors. Introducing the Kohn-Sham orbitals directly in the energy functional so that the self-energy of the Hartree term and the exchange part cancel out exactly can solve this problem. The first and still usable proposal of this was the self-interaction corrected LDA (SIC-LDA) by Perdew and Zunger in 1981 [17].

Gradient expansions were considered already in the original work of Hohenberg and Kohn [2]. However, it took a couple decades of research until the nowadays flourishing family of generalized gradient approximations (GGAs) came into existence [18, 19]. They take into account also the local density gradient at each point as

$$E_{xc}^{\mathrm{GGA}} = \int n(\boldsymbol{r}) \varepsilon_{\mathrm{xc}}^{\mathrm{GGA}}(n(\boldsymbol{r}), \nabla n(\boldsymbol{r})) d^3r. \tag{3.9}$$

When determining the function $\varepsilon_{\mathrm{xc}}^{\mathrm{GGA}}(n, \nabla n)$, a whole ensemble of exact constraints is applied to the gradient expansion. In a few GGAs, some free parameters also remain to be fixed by experiments. In the course of time, advanced implementations of GGA have been developed, the most popular of which is the PBE (Perdew-Burke-Ernzerhof) [20]. A further extension are the meta-GGAs (MGGAs) [21], where also the kinetic energy density is taken into account.

The GGAs and MGGAs improve the shortcomings of LDA, reaching the chemical accuracy in some cases, but still struggle more or less with the same problems. To improve the performance of the DFT methods, non-local functionals such as BLYP (Becke-Lee-Yang-Parr) [19, 22] have been developed. Hybrid functionals [1] such as B3LYP [23–25] include a fraction of the exact exchange of the

Hartree-Fock theory, calculated by using the Kohn-Sham orbitals. Even though the hybrid functionals often overcome the problems of LDA and (M)GGAs, they usually have a highly empirical character which, in a strict sense, is in conflict with the principles of DFT. Another, promising group of advanced functionals are the orbital-dependent functionals [26].

3.3 Pseudopotentials and basis sets

In practice, the Kohn-Sham orbitals are often expanded in a finite set of basis functions χ_μ when solving the Kohn-Sham equations numerically. Cartesian Gaussians are the most used basis functions. Other common choices are Slater type orbitals, plane waves or piecewise defined functions on a numerical grid.

When the Kohn-Sham orbitals are approximated by a linear combination of basis functions, the Kohn-Sham equations become a finite-dimensional matrix equation. Thus all operators become finite matrices and all the matrix elements are integrals of the type

$$X_{\mu\nu} = \int \chi_\mu(\boldsymbol{r}) X[n] \chi_\nu(\boldsymbol{r}) d^3r. \tag{3.10}$$

The processing of such integrals is one of the main parts of practically all the DFT calculations. For the diagonalization of the ensuing eigenvalue problem there exists efficient methods of numerical linear algebra.

Instead of treating all the electrons separately, pseudopotentials are often used in electronic-structure calculations especially for solids. In this approach, only the chemically active valence electron states are considered explicitly, which results in considerable reduction in the basis set size. The core electrons are treated together with the nuclei as rigid ion cores.

The use of pseudopotentials reduces the number of electron states to be considered. But the most important simplification is the substitution of all-electron valence wave functions, which oscillate rapidly near the nuclei, by smooth pseudo wave functions. The presentation of pseudo wave functions requires much less basis functions than that of the all-electron wave functions.

The pseudopotentials are derived from atomic reference states. In norm-conserving pseudopotentials, pseudo and all-electron valence eigenstates are required to be identical outside the core cutoff radius r_c. The larger the core cutoff radius, the softer the potential. That is, the calculations converge faster but are less accurate in reproducing realistic features in different chemical environments.

Chapter 4

Time-dependent density-functional theory

The DFT formalism presented in the previous Chapter cannot be used to extract information on excited states. The reason is that even though the Hohenberg-Kohn theorem holds, it is only an existence proof and does not provide a practical way to write the excitation energies as a functional of the ground state density. However, the excited states can be successfully studied by an analogue to DFT, namely by the time-dependent density-functional theory (TDDFT).

Before discussing the TDDFT methods, we summarize other approaches that can be used to access the excited-state properties of matter. To begin, the unoccupied Kohn-Sham states can be used as very crude estimates of the excited single-particle states. Actually, the Kohn-Sham eigenstates (wave functions and eigenvalues) do not represent any physical quantities. The highest occupied ground state energy makes an exception as its eigenvalue represents the first ionization potential.

More advanced methods to access the excited state properties by the ground-state theory are, among others, Δ_{SCF} (delta self-consistent field) [27] and ensemble DFT (see Ref. [28] and references therein). However, these approaches are not very accurate.

Beside the DFT-based methods, there exist several approaches for accurate quantum mechanical calculations of excitation energies. The most important ones are the configuration interaction (CI) method [29, 30], quantum Monte Carlo (QMC) simulations [31, 32], coupled-cluster (CC) expansions to many-body perturbation theory [33] (MP2 etc.) and the Green's function method based on the GW approximation [34, 35]. These methods do not have the advantageous scaling property of DFT so they can only be applied to small systems except for the GW-Bethe-Salpeter equation method (GW-BSE), which has been developed

actively in recent years and offers an alternative to the TDDFT formalism especially for extended solid-state systems [36]. There is also evidence that such many-body perturbation theory methods and TDDFT could be developed hand in hand or even combined, because they share same kinds of challenges [37].

4.1 Extension of DFT to the time regime

Let us consider the time-dependent, non-relativistic Schrödinger equation

$$i\frac{\partial\Psi(\{\boldsymbol{r}_i\},t)}{\partial t} = \widehat{H}(\{\boldsymbol{r}_i\},t)\Psi(\{\boldsymbol{r}_i\},t), \tag{4.1}$$

where the initial wave function Ψ_0 is given. By this equation we want to describe N mutually interacting electrons in a time-dependent external potential. It should be noted that this problem differs significantly from that of Eq. (3.1) for the ground state. Mathematically, it is an initial value problem whereas the ground-state Schrödinger equation is a boundary value problem. However, it turns out that an analogous statement to Hohenberg-Kohn theorem can be proven for the time-dependent problem. Namely, the Runge-Gross theorem [6] states that there is a one-to-one correspondence between the time-dependent external potential $v_{\text{ext}}(\boldsymbol{r},t)$ and the time-dependent electron density $n(\boldsymbol{r},t)$.

This extension to time-domain is nontrivial and its proof is divided into two parts as follows. Let us consider two electron densities, $n(\boldsymbol{r},t)$ and $n(\boldsymbol{r}',t)$, evolving from a common initial state under the influence of two external potentials, $v_{\text{ext}}(\boldsymbol{r},t)$ and $v_{\text{ext}}(\boldsymbol{r}',t)$, that differ by more than a purely time-dependent function. Firstly, it can be shown that v and v' produce different current densities j and j', using the equation of motion for the current densities. In the second part, the different current densities are shown to produce different electron densities by the continuity equation. The time-dependent potentials are required to be Taylor expandable around the initial time in the original proof. This is a mild condition that is certainly true for all physical potentials.

As in the time-independent case, we can now solve the Schrödinger equation and get all the properties of the system if we know the electron density. It is straightforward to construct a time-dependent Kohn-Sham scheme. The time-dependent Kohn-Sham equations attain the form

$$i\frac{\partial\psi_j(\boldsymbol{r},t)}{\partial t} = \Big(-\frac{\nabla^2}{2} + v_{\text{KS}}[n](\boldsymbol{r},t)\Big)\psi_j(\boldsymbol{r},t), \tag{4.2}$$

where

$$v_{\text{KS}}[n](\boldsymbol{r},t) = v_{\text{ext}}[n](\boldsymbol{r},t) + v_{\text{H}}[n](\boldsymbol{r},t) + v_{\text{xc}}[n](\boldsymbol{r},t) \tag{4.3}$$

The Hartree term remains the same as in the ground-state case in Eq. (3.6). As challenging as it is to find a good exchange-correlation functional for the ground-state as described in Sec. 3.2., the time dependence brings yet another problem to it. Namely, the potential at $(\boldsymbol{r}, t)$ depends not only on the density $n(\boldsymbol{r}, t)$ but on all $n(\boldsymbol{r}, t')$ for $0 \leq t' \leq t$. The potential thus has a causal connection to the history of the density. In short, the system has memory.

The simplest way to handle this situation is to ignore the memory effect and assume that the functional is local in time. This is called the adiabatic approximation, which is expressed as

$$v_{\mathrm{xc}}^{\mathrm{adia}}[n](\boldsymbol{r}, t) = v_{\mathrm{xc}}[n(t)](\boldsymbol{r}). \tag{4.4}$$

For this approximation to be valid, the time-dependent potential must change slowly, that is, adiabatically.

The adiabatic approximation works surprisingly well in practice, also in many cases where its validity is all but self-evident. Today, almost all the applications of TDDFT use the adiabatic approximation. By far the most common approximation within TDDFT is the adiabatic LDA (ALDA). More accurate approximations with memory effects are being developed [38]. For example, the Keldysh formalism allows to construct exchange-correlation potentials with memory via its relation to non-equilibrium Green functions [39]. A related question arising with approximations containing memory is their initial-state dependence [38].

There are two parallel alternatives for calculating the optical spectra within TDDFT. They are the linear response formalism, which is presented in Sec. 4.2, and direct propagation in time presented below.

By utilizing the time-dependent Kohn-Sham equations the electronic excitations can be accessed as follows. The system under study is weakly perturbed at $t = 0$ at all frequencies. This can be expressed as

$$\psi_j(\boldsymbol{r}, \delta t) = e^{i\kappa\gamma}\psi_j(\boldsymbol{r}, 0), \tag{4.5}$$

where $\gamma = x, y, z$ and κ is a small momentum given to the electron. Then the system is let to evolve in time by propagating the time-dependent Kohn-Sham equations. To get the optical absorption spectrum of a finite system, the dipole moment of the system is recorded as a function of time and Fourier-transformed to frequency space. More specifically, the dynamical polarizability $\alpha_\gamma(\omega)$ is essentially the Fourier transform of the dipole moment p as

$$\alpha_\gamma(\omega) = \frac{1}{\kappa}\int dt e^{i\omega t}\big(p(t) - p(0)\big) = -\frac{1}{\kappa}\int d^3r\gamma\delta n(\boldsymbol{r}, \omega), \tag{4.6}$$

where $\delta n(\boldsymbol{r}, \omega)$ denotes the density deviation from the ground state. Finally, the photoabsorption cross section is proportional to the imaginary part of the

dynamical polarizability as

$$S(\omega) = \frac{2\omega}{3\pi}\mathrm{Im}\sum_{\gamma}\alpha_{\gamma}(\omega), \tag{4.7}$$

where $S(\omega)$ is the dipole strength function and the average over all the three spatial components has been taken. In this procedure, the Thomas-Reiche-Kuhn f-sum rule,

$$N = \int d\omega S(\omega), \tag{4.8}$$

is obeyed.

The approach presented above was first demonstrated by Yabana and Bertsch in 1996 [40]. This method can be easily utilized also in the cases of nonlinear response or large perturbations. Typical examples are high-harmonic generation (emission of radiation at odd-integer multiples of the frequency of the applied laser field) or above-threshold ionization in intense laser fields.

However, there are some cases where the TDDFT method fails in describing the electronic excitations. For example, the Rydberg states are not reproduced when using the adiabatic LDA [41]. This is mainly due to the wrong asymptotic behaviour of the exchange-correlation potential in the local-density and gradient-corrected approximations. When the system is extended as, for example, in long conjugated polymers, the situation gets even worse. Generally, the use of the TDDFT method to calculate the optical spectra is currently restricted essentially to finite systems. Different approaches have been studied to correct the shortcomings of the method in extended systems, see Ref. [37]. Another shortcoming of the TDDFT method is that it cannot describe charge-transfer excitations easily. The third problem is the final-state interactions such as those between electrons and holes that make excitons (bound states), cf. Rydberg states [36].

4.2 Linear-response formalism

In order to get the linear excitation spectrum, it is also possible to use the linear-response theory to evaluate directly the susceptibility χ. The first complete formulation of the response theory used today was done in 1985 [42].

The starting point for a linear-response calculation is a ground-state DFT calculation, including a sufficient number of unoccupied Kohn-Sham states. The first-order correction to the ground-state density must produce the same density

change in both the interacting and the Kohn-Sham system,

$$\begin{aligned}\delta n(\boldsymbol{r},t) &= \int dt' \int d^3r' \chi(\boldsymbol{r},\boldsymbol{r}',t-t')\delta v_{ext}(\boldsymbol{r}',t') \\ &= \int dt' \int d^3r' \chi_{KS}(\boldsymbol{r},\boldsymbol{r}',t-t')\delta v_{KS}(\boldsymbol{r}',t'),\end{aligned} \tag{4.9}$$

where χ and χ_{KS} are the linear density-response functions of the interacting system and the Kohn-Sham system, respectively. To get the relation between the potentials, we recall Eq. (4.3), which gives

$$\delta v_{KS}(\boldsymbol{r},\omega) = \delta v_{ext}(\boldsymbol{r},\omega) + \int d^3r' \frac{\delta n(\boldsymbol{r},\omega)}{|\boldsymbol{r}-\boldsymbol{r}'|} + \int d^3r' f_{xc}(\boldsymbol{r},\boldsymbol{r}',\omega)\delta n(\boldsymbol{r}',\omega) \tag{4.10}$$

in the frequency space. Above, we have introduced the Fourier transform of the time-dependent kernel

$$f_{xc}(\boldsymbol{r},\boldsymbol{r}',t-t') = \frac{\delta v_{ext}(\boldsymbol{r},t)}{\delta n(\boldsymbol{r}',t')}. \tag{4.11}$$

By Fourier transforming Eq. (4.9) to the frequency space and using linear perturbation theory, the Dyson-like equation

$$\begin{aligned}\chi(\boldsymbol{r},\boldsymbol{r}',\omega) &= \chi_{KS}(\boldsymbol{r},\boldsymbol{r}',\omega) + \int d^3r'' \int d^3r''' \chi_{KS}(\boldsymbol{r},\boldsymbol{r}'',\omega) \\ &\quad \times \Big(\frac{1}{|\boldsymbol{r}''-\boldsymbol{r}'''|} + f_{xc}(\boldsymbol{r}'',\boldsymbol{r}''',\omega)\Big)\chi(\boldsymbol{r}''',\boldsymbol{r}',\omega)\end{aligned} \tag{4.12}$$

is obtained for the χ of the interacting system.

The full solution of Eq. (4.12) is still numerically difficult. Following the notation by Casida [43] and Petersilka [44], the problem can be turned into solving the eigenvalue problem

$$\boldsymbol{Q}\boldsymbol{F}_I = \Omega_I^2 \boldsymbol{F}_I \tag{4.13}$$

after a considerable amount of algebra. Above, Ω_I denotes the Ith excitation energy and the eigenvectors $\boldsymbol{F}_I$ can be used to obtain the oscillator strengths. The matrix elements of $\boldsymbol{Q}$ are given by

$$\boldsymbol{Q}_{ij,kl} = \delta_{i,k}\delta_{j,l}\omega_{kl}^2 + 2\sqrt{\omega_{ij}}\boldsymbol{K}_{ij,kl}\sqrt{\omega_{kl}}, \tag{4.14}$$

where i and k run over the unoccupied states and j and l over the occupied states. $\omega_{ij} = \varepsilon_i - \varepsilon_j$ are the differences between the energy eigenvalues of the single-particle states. $\boldsymbol{K}$ is a coupling matrix with elements

$$\boldsymbol{K}_{ij,kl}(\omega) = \int\int \psi_i^*(\boldsymbol{r})\psi_j^*(\boldsymbol{r})\Big(\frac{1}{|\boldsymbol{r}-\boldsymbol{r}'|} + f_{xc}(\boldsymbol{r},\boldsymbol{r}',\omega)\Big)\psi_k(\boldsymbol{r}')\psi_l(\boldsymbol{r}')d^3r d^3r'. \tag{4.15}$$

Above, adiabaticity has been assumed. Consequently, the matrix $\boldsymbol{Q}$ is independent of the excitation energy. For exchange-correlation functionals with memory this does not hold and the non-linear eigenvalue problem, $\boldsymbol{Q}(\Omega_I)\boldsymbol{F}_I = \Omega_I^2\boldsymbol{F}_I$, has to be solved self-consistently.

Several exchange-correlation kernels f_{xc} have been proposed during the years (see Ref. [36] for a listing). There are two approaches to search for a good exchange-correlation kernel f_{xc}. One can first find a good time-dependent exchange-correlation potential to derive the kernel from, or directly search for a good exchange-correlation kernel.

The standard exchange-correlation potentials are adiabatic, leading to very simple kernels. Recently, the development of improved linear-response kernels derived from many-body perturbation theory has been successful [4, 37]. Two different classes of such approaches are being developed. The first one is based on approximated exchange-correlation functionals or on the Sham-Schlüter equation, which impose the many-body density equal the DFT one. The second class assumes the Kohn-Sham and quasiparticle states to be the same, targeting to a kernel which can account for the electron-hole interaction and the excitonic effects provided by the Bethe-Salpeter equation. This development brings TDDFT a promising method to calculate the electronic spectra even for extended systems [4].

4.3 Computational considerations

For few-atom clusters and small molecules, the linear response formalism is the ideal method because the prefactor of the real-time propagation is considerably large. A typical calculation requires $O(10000)$ time-steps of $O(0.001)$ fs each. However, the computational cost of the linear methods increases roughly as N^3. The bad scaling limits their usability to the accurate treatment of systems with only a few dozen atoms taking into account the current computational resources. The linear scaling of the real-time propagation is thus overwhelmingly favourable for systems with more than a few tens of atoms. For large systems, the bottleneck of linear-response methods is the calculation of the unoccupied Kohn-Sham states. Namely, the recommended number of fully converged unoccupied states is at least 4–8 times the number of occupied states.

Nowadays, a linear-response TDDFT method, typically the Casida method, is included in all advanced computational chemistry packages that are based on DFT. The only widely available real-time implementation of TDDFT has been the OCTOPUS code [45, 46]. Recently, another electron-structure package, namely the GPAW [47, 48] has been extended to include also the real-time TDDFT.

In the following some technical details of the implementation of the OCTOPUS are shortly reviewed. The same information mainly holds also for the GPAW code.

The time-dependent Kohn-Sham equations are solved on a three-dimensional real-space grid. The real-space TDDFT method does not support artificial periodicity in contrast to supercell calculations in the momentum space. In other words, only localized structures such as molecules and clusters can be calculated in the real-space formalism. The wave functions and electron density become zero at the boundary of the grid domain. The key parameter that governs the accuracy of the calculations is the grid spacing, whose value is usually about 0.2–0.3 Å. Charged systems can be treated with no extra difficulty.

The kinetic energy operator is approximated by a high-order finite difference expansion on grid points. The different time-propagation methods of the time-dependent Schrödinger equation that are implemented in OCTOPUS are discussed in Ref. [49].

Currently, about 500 electronic states is the maximum computationally manageable system size in our real-time calculations. The pseudopotential approach is used to reduce the number of electrons by removing the chemically inert core electrons. In all the work reported in this Thesis, the Troullier-Martins norm-conserving pseudopotentials are used [50]. The GPAW code uses projector augmented waves (PAW) potentials [51] instead.

In all previous considerations, the spin variables are omitted for simplicity. However, it is straightforward to derive all the formalism and computer programs for the two spin components.

Chapter 5

Materials and results

5.1 Fullerenes

The flourishing research of different carbon nanostructures started by the discovery of fullerenes by Kroto and coworkers in 1985 [52]. The first nanotubes were produced in 1991 [53], though since the 1950's, previous experimental evidence of them existed. Later, various other carbon structures have been produced and studied, for example onions, cones and tubules [54]. The latest major discovery is the graphene synthesis [55]. A recent Finnish discovery are the so the called nanobuds which are fullerenes bonded to carbon nanotubes [56]. Here, we concentrate on selected fullerenes and fullerene derivatives.

The fullerene structure can be modified in a variety of ways. The size can be varied from C_{20} to cages that consist of hundreds of atoms. What is even more important, the fullerenes can be doped endohedrally, exohedrally and substitutionally. This makes them a flexible material which can be functionalized and whose properties can be tuned. Many potential uses have been suggested for fullerenes, for example, as hydrogen storage or solar cell material. Medical applications such as drug delivery, use as lubricant and even as rocket fuel have also been suggested, but no true commercial applications have appeared so far. [57]

5.1.1 Small fullerenes

The buckminsterfullerene C_{60} consists of 12 pentagons and 20 hexagons and is the smallest fullerene which follows the isolated pentagon rule (IPR). However, also many highly curved and strained smaller fullerenes with less hexagons are stable down to the smallest fullerene C_{20}, which is built of solely 12 pentagons. The crossover from chain or ring structures to fullerenes as the most stable C_n isomers takes place around $n = 26$–30 (see, e.g., Ref. [58]).

Soon after the discovery of the buckminsterfullerene, fullerenes with a wide mass range were routinely produced by gas-phase methods. However, their synthesis and isolation in macroscopic quantities has been extremely difficult. So far, the only small fullerene produced in the solid state is C_{36} [59].

The structures and ground state properties of small fullerenes have been studied extensively by computational methods (see, e.g., Refs. [60, 61]). C_{20}, C_{28}, C_{36}, C_{44}, C_{50} and especially C_{32} have been in the scope because they are produced in abundance in gas phase experiments.

The energies of the different isomers are often so close to each other that various theoretical calculations give inconsistent predictions as the ground state isomer. After the smallest fullerene, C_{20}, was synthesized in 2000 [62], computational optical spectroscopy, more precisely the real-time TDDFT method, was used to demonstrate its capability of distinguishing between the fullerene, cage and bowl isomers of C_{20} [63]. Linear response TDDFT has been used to calculate the optical spectrum of the fullerene derivative $C_{50}Cl_{10}$ [64], which was the first fullerene derivative that was synthesized in milligram quantities in 2004 [65].

In Publication I, a series of low-energy fullerene structures in the size range of C_{20}–C_{60} is examined. Their absorption spectra are observed to have features that can be connected with the geometry of the fullerenes. Firstly, the main π-π^* transition shifts from about 4.7 eV to 5.8 eV as the size increases from C_{20} to C_{60} as shown in Fig. 5.1. Secondly, the symmetry decreases and different bond lengths appear, increasing the general complexity of the absorption spectrum. Thirdly, the degeneracy of the main low-energy transition disappears and the main excitation peak splits into clear subpeaks when the cage geometry differs from the spherical shape. This is the case especially for the D_{6h} isomer of C_{36}, which has the form of an elongated cage.

The two common functionals, LDA and PBE, are compared. The results are practically identical except for a small constant shift of the LDA results to higher energies. This is a commonly known feature due to the stronger bonding in the LDA calculations.

After our work, the optical properties of some small fullerenes are studied in Ref. [66]. They compare the GW-BSE and diffusion QMC results with the TDDFT calculations for the lowest-energy excitations.

5.1.2 Silicon-doped fullerenes

Silicon is the neighbouring element of carbon in the fourth row of the periodic table of elements. This raises the question whether carbon can be substituted by silicon in its nanostructures. Pure silicon fullerenes are known to be unstable due to the lack of sp^2 bonding for silicon, but extensive experimental and theoretical

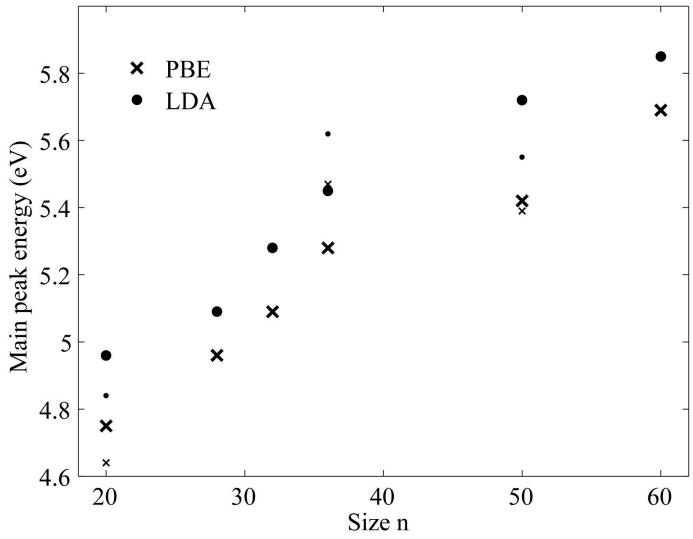

Figure 5.1: Energy of the main peak in the absorption spectrum of the studied small fullerenes in the range of $C_{20} - C_{60}$. The smaller markers represent isomers with slightly higher energy in the cases where two minimum energy structure candidates are studied.

investigations have revealed that small metal-encapsulating Si-fullerenes up to Si_{20} may be stable (see Ref. [67] and references therein). Another branch of activity deals with the carbon-silicon heterofullerenes.

Experimental observations have confirmed the existence of $C_{60-n}Si_n$ heterofullerenes up to about $n = 12$ [68]. On the theoretical side, the structure and electronic properties of heterofullerenes have been investigated since late 1990's, starting from the fullerenes with one and two dopant silicon atoms (see, for example, Ref. [69] and references therein). Recently, the upper limit of the doping has been examined. First-principle molecular dynamics simulations predict that thermal stability is maintained up to $n = 20$ [70] and that charged structures of $C_{30}Si_{30}$ could be realistic [69]. In all the studies, carbon and silicon atoms are found to prefer arrangements with separate regions.

In Publication I, the low-energy isomers of C_{60}, $C_{59}Si$, $C_{58}Si_2$, $C_{54}Si_6$ and $C_{48}Si_{12}$ are considered. The choice of structures is based on previous studies, especially on Refs. [71, 72]. The structures of the studied silicon-richest fullerenes are shown in Fig. 5.2.

We observe that already one dopant atom introduces significant changes in the absorption spectrum. Especially, the optical gap is lowered and certain absorp-

tion appears in the visible range. The different isomers of $C_{58}Si_2$ show some characteristic spectral properties. The more heavily doped structures are less symmetric and tend to have rather indistinguishable spectra.

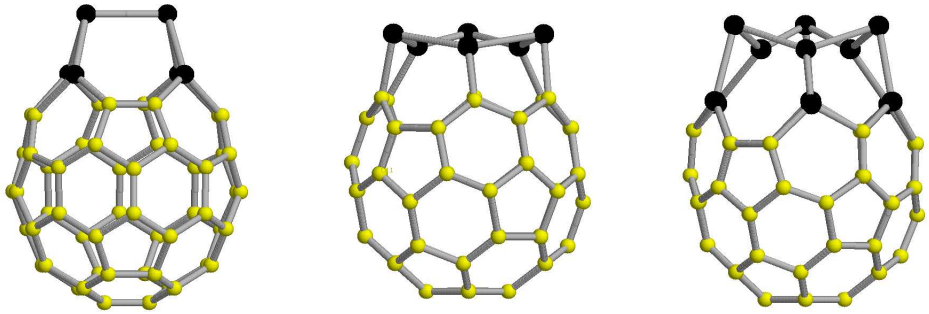

Figure 5.2: Example structures of the studied Si-doped carbon fullerenes. The big black dots represent the silicon atoms.

5.1.3 Boron nitride fullerenes

The discovery of low-dimensional carbon allotropes raised the question whether such nanostructures could be entirely based also on other elements or compounds. The most natural choices are the elements in the same column of the Periodic Table (for example, Si) or the neighbouring elements in the same row, that is, boron and nitride. Especially, the chemistry of boron nitride (BN) has significant similarity to carbon, which makes the existence of its fullerene and nanotube structures probable.

Indeed, the first BN nanotubes [73], nested cages [74] and fullerenes [75, 76] were experimentally produced already in the 1990's. Despite the effort in developing various production methods, the efficiency and controllability of the synthesis remains low for BN nanostructures. Thus, atomistic simulation methods can provide considerable insight in their structure determination and prediction of properties.

The computational studies on BN fullerenes have so far focused mainly on the structural stability of different cage sizes and morphologies (see Refs. 9–18 of Publication II). Especially, the different possible structures of $B_{24}N_{24}$ have been under study because $B_{24}N_{24}$ can be experimentally produced in unexpected abundance.

To the best of our knowledge, Publication II presents the first calculations considering the optical properties of BN fullerenes. We have calculated the optical absorption spectra for a selected series of BN fullerenes within the size range from $B_{12}N_{12}$ to $B_{36}N_{36}$ and containing different isomers for some of the fullerenes.

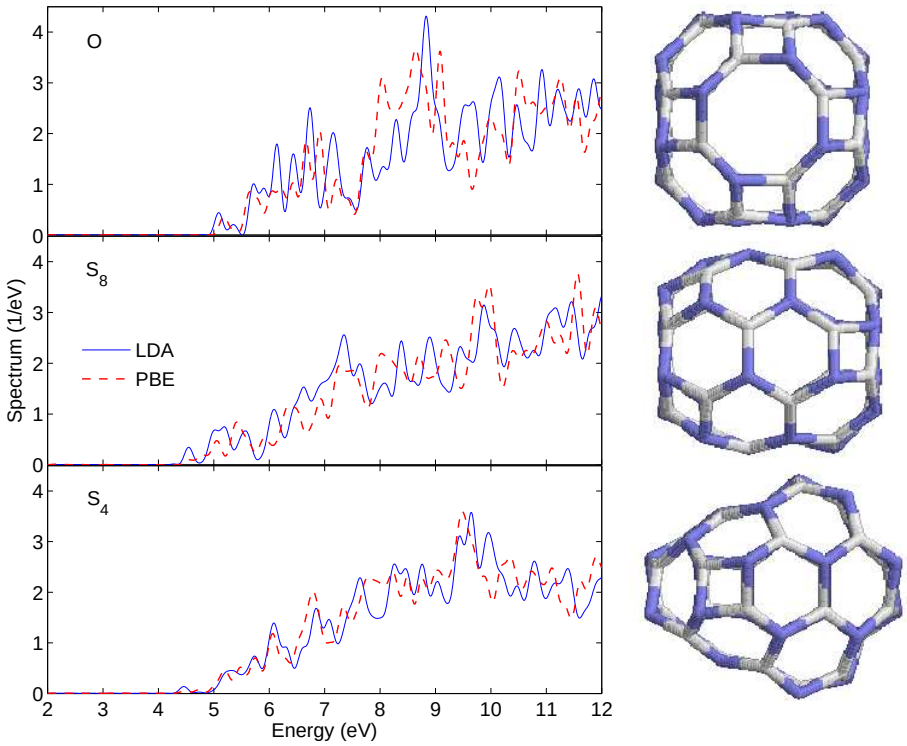

Figure 5.3: Calculated photoabsorption spectra and structures of the three studied isomers of $B_{24}N_{24}$.

Figure 5.3 shows an example of the obtained results. The calculated absorption spectra of the three almost isoenergetic isomers of $B_{24}N_{24}$ are shown together with the illustrations of their optimized structures. Some clear differences between the spectra are observed. To some extent, they can be associated with the geometry and the amount of symmetry in the isomers. The LDA and PBE functionals are also compared and no significant differences are observed for BN fullerenes.

After our work, published articles on BN fullerenes consider, for example, structural properties [77, 78] and doping with metal atoms [79] which are commonly present during the synthesis of BN nanostructures. During the very last years, boron nitride nanotubes have attracted much more interest than boron nitride fullerenes. Besides boron nitride, pure boron and aluminum nitride fullerenes have been addressed in recent research. Aluminum nitride fullerenes are predicted to have very similar structures as boron nitride fullerenes [80]. Recently, the existence of a stable boron fullerene B_{80} with a very similar structure to that of C_{60} has been predicted [81] and the optical properties of different hypothetical

boron fullerenes have been calculated using the real-time TDDFT [82].

Apart from the abovementioned materials, a wealth of other inorganic fullerene- and nanotube-like materials has been synthesized (for a review, see Ref. [83]).

5.2 Silicon nanocrystals

The quest of silicon-based optically active devices such as lasers has shown to be a challenging task. The indirect optical gap of pure bulk silicon makes it an unsuitable material for active optical applications, but different low-dimensional silicon nanostructures seem promising for various optoelectronic devices. The use of silicon in photonics is also strongly motivated by practical reasons such as the low cost and the easy manufacturability of the material. For reviews of the material, see Refs. [84–87].

A major starting boost in silicon photonics took place in 1990 when light emission from porous silicon in room temperature was demonstrated [88]. Another breakthrough happened in 2000 by the demonstration of optical gain in silicon nanocrystals [89]. Since then, the optical properties of silicon nanocrystals have been studied extensively in experiments, but still the exact atomic structures and their relations to the optical properties are unclear (see, e.g., [90, 91]).

Especially, the origin of the photoluminescence in nanosilicon is still not understood and is under debate. Several mechanisms have been proposed, the most probable of which are the quantum confinement effect, different defects in the surface such as oxygen defects or dangling bonds, and suboxide formation. Other proposals include nanocrystal surface states [92], molecular functional groups such as silane chains [93] and structural disorder.

In recent years, a lot of computational study has been carried out on the optical properties of small free-standing silicon nanocrystals. The different structures include hydrogenated crystals, e.g. [84, 94], hydroxidated crystals [84, 95] and crystals with surface oxygen defects [84, 96–98]. Especially, the double-bonded oxygen atoms on the surface are connected with increased optical activity.

Since 2003, the computationally more challenging case of small silicon nanocrystals embedded in silica has been addressed in a few studies [99, 100]. Interestingly, the defects do not seem to play an important role in this case [101]. Also the effect of amorphization has been considered [102]. The structures of larger crystals in silica can be calculated using, for example, the molecular dynamics (MD) simulation methods [103].

In Publication III, the effect of the embedding silica on the absorption characteristics of the silicon nanocrystals is addressed. A systematic study of different

crystal sizes from Si_5 to Si_{47} is presented. Hydrogen passivation and an embedding silicon oxide layer are considered in each case. The structure of the crystal is set up as a spherical perfect quartz lattice which is embedded in the regular oxide structure, and then a structure optimization is done for the whole structure. The system retains its symmetric structure with no dangling bonds or surface defects. The structure is intentionally chosen simple and defect-free in order to extract the purely size-dependent effect. The thickness of the oxide is one or two layers and it is limited by the increasing computational cost of larger systems.

The main result of the study is shown in Fig. 5.4, where the minimum absorption energy is plotted as a function of crystal size. An interesting size dependent behaviour is observed. For the hydrogen-passivated crystals, a trend of decreasing optical gap with the increasing crystal size is seen, in full accordance with previous studies. For the oxygen-embedded case, qualitatively totally different behaviour is found. A roughly constant absorption onset at about 3 eV is observed for all sizes except for the smallest crystal which is so small that it does not have a proper surface region. The absorption edge is thus in the blue end of the visible range and it is clearly lowered compared to the hydrogen-passivated case. A possible explanation for this behaviour is associated with the localization of the HOMO states in the vicinity of the nanocrystal-oxide interface.

A further investigation with the inclusion of defects or other structural distortion to the studied systems would be an interesting task. Another room for further improvement is the treatment of oxide. Namely, periodic simulation cells are not available in the current implementations of the real-time TDDFT method (see Ch. 4). By applying periodic boundary conditions, the important impact of the crystal orientation could also be investigated.

5.3 Silver clusters and their hybrid systems

Extensive experimental and theoretical research has revealed that small metal nanoparticles exhibit interesting optical properties that vary as a function of their size. The absorption spectra of small silver clusters have been traditionally measured embedded in rare-gas matrices (e.g., [104]). However, many of the potential applications of silver nanoparticles are based on their functionalization by a complex environment.

The current status of the synthesis and structural characterization of small metal nanoclusters is reviewed, e.g., in Ref. [105]. The structure and properties of few-atom silver clusters have also been intensively studied computationally for several decades. The optical absorption of small silver clusters within the TDDFT was first calculated in 1999 [106], followed by many other works, for example, that of Ref. [107]. In recent years, the studied system sizes have grown from less than

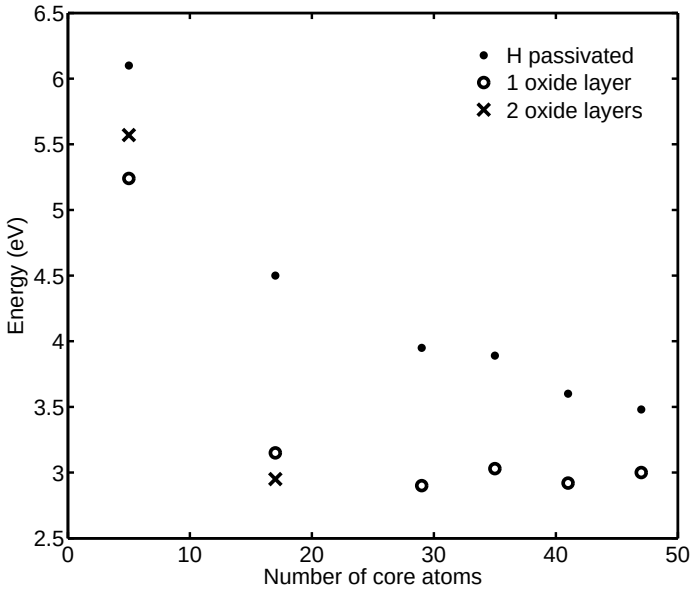

Figure 5.4: Calculated optical gap energies of hydrogen passivated Si-nc's (dots), Si-nc's with one SiO_2 layer (circles), and Si-nc's with two SiO_2 layers (crosses).

ten atoms to about two dozens of atoms. In addition, comparisons between the TDDFT and the GW methods have been made [108] and the effect of semicore states has been addressed [109].

The original motivation to our study of hybrid structures of silver clusters arose from the work reported in Ref. [110]. In this study, Díez and coworkers found out that the silver nitrate and poly(methacrylic acid) (PMAA) form a pink solution in certain conditions. In a further analysis, the clusters in the solution were measured to exhibit strong luminescent properties. The particles were found to be few-atom clusters, but the atomic structure of the system and the origin of the luminescence remained unclear.

Similar experimental results have been recently reported also in Ref. [111]. The complex formation of silver with PMAA brushes has been studied in Ref. [112], and descriptions of encapsulated dendrimer- and peptide few-atom silver clusters can be found, for example, in Ref. [113] and in references therein.

Computational studies of hybrid silver-polymer systems are rare. Mitrić *et al.* have studied tryptophan-silver hybrid systems [114, 115]. We have studied the smallest silver clusters Ag_1–Ag_3. Three different types of structures are considered: pure clusters, clusters attached to one PMAA chain and clusters attached

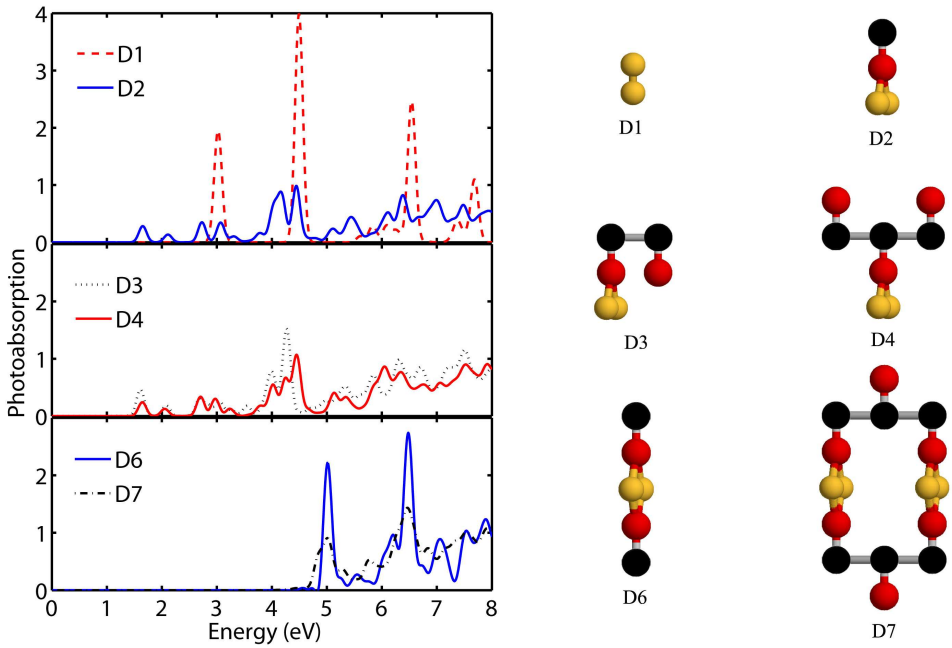

Figure 5.5: Calculated optical absorption spectra of different structures containing the silver dimer cluster. D1 is the pure cluster, D2–D4 are clusters attached to one polymer chain and D6 and D7 are clusters between two polymer chains. On the right, schematic illustrations of the structures are given. Black, dark red and light yellow balls represent the PMAA polymer units, their carboxylate groups and silver atoms, respectively. The shown bond lengths and bond angles do not correspond to the calculated values.

to two PMAA chains. In the two latter cases, the silver clusters are bonded to the oxygen atoms of the chemically active part of the PMAA ion, namely the carboxylate group. In addition, pure PMAA is also considered as a reference.

Our real-time TDDFT and Casida calculations reveal that the presence of polymer causes significant changes in the electronic structure and thereby also in the absorption spectra of the silver clusters. As an example, Fig. 5.5 shows the calculated absorption spectra of the studied silver dimer structures. One can observe that the absorption edge is lowered by about 1.5 eV in the silver cluster-PMAA chain structures (D2–D4) compared to the pure cluster (D1). The low-energy absorption is associated with the local spin polarization in the vicinity of the silver clusters. The opposite effect, namely quenching of the lowest energy excitations of the dimer, takes place in systems with two chains (D6–D7).

As additional material related to the study presented above, we want to show

some unpublished results on mutually interacting silver nanoclusters. The studied structures are again the smallest silver clusters Ag_1–Ag_3. The idea is to study the mutual interaction of silver clusters only, without any effect of other structures which could in practice provide the environment for such stable silver cluster pairs. Therefore, two such silver clusters are placed at the mutual distance d, which is varied from 3 Å to infinity (corresponding to a separate single cluster calculation). This arrangement is somewhat artificial in the sense that such structures are not even local energy minima. It should also be noted that TDDFT with adiabatic approximation has difficulties in describing the excitations of dissociating molecules [116].

The absorption spectra are calculated using the Casida method. The PBE exchange-correlation functional is used (but the LDA exchange-correlation kernel is used because its PBE variant is lacking in the current version of OCTOPUS). A grid spacing of 0.23 Å and a simulation radius of 8 Å around each atom are chosen as the key parameter values.

The ground state calculation shows that for the odd-spin clusters Ag_1 and Ag_3, the orientation of the spins in the two clusters is parallel for the studied distances $d \geq 5$ Å. At shorter distances, no local spin polarization takes place. Some of the calculated properties of the systems are collected in Table 5.1. We can see that the optical gap, that is, the minimum optical absorption energy, shows a vaguely similar trend as the HOMO-LUMO gap, especially for the trimers. However, the optical gaps are systematically considerably larger than the HOMO-LUMO gaps. All the energies shown there have an error marginal of a few tenths of eV. Especially, the values of the binding energies are intentionally given in an inaccurate form to underline that these results are not of chemical accuracy.

The calculated spectra are shown in Fig. 5.6. For the dimers (Fig. 5.6 (b)), the absorption spectra change smoothly between the extreme distances 3 Å and infinity. On the contrary, the shifting of the absorption edge to lower energies at the intermediate distances is observed for the monomers (Fig. 5.6 (a)) and especially strongly for the trimers (Fig. 5.6 (c)). For monomer and trimer pairs, the behaviour of the absorption edge, as well as that of the HOMO-LUMO gap shown in Table 5.1, reflects the change in the total spin of the cluster pair.

Table 5.1: Calculated properties of silver cluster pairs with varying distances d. E_b denotes the binding energy per atom compared to a single silver atom.

Cluster	d	E_b	HOMO-LUMO	Optical gap
Ag	3 Å	0.9	1.61	3.06
	4 Å	0.3	0.75	2.39
	5 Å	0.03	0.44	3.59
	6 Å	0.01	0.65	3.65
	8 Å	0.1	0.75	3.69
	inf	–	0.76	4.29
Ag_2	3 Å	1.0	0.19	2.22
	4 Å	1.0	1.22	3.40
	5 Å	0.9	1.73	3.36
	6 Å	0.9	1.93	3.33
	8 Å	1.0	2.02	3.31
	inf	0.9	2.04	3.30
Ag_3	3 Å	1.4	0.10	2.31
	4 Å	1.2	0.13	1.73
	5 Å	1.0	≈ 0.00	0.87
	6 Å	1.0	0.19	2.36
	8 Å	1.2	0.29	2.39
	inf	1.0	0.31	2.77

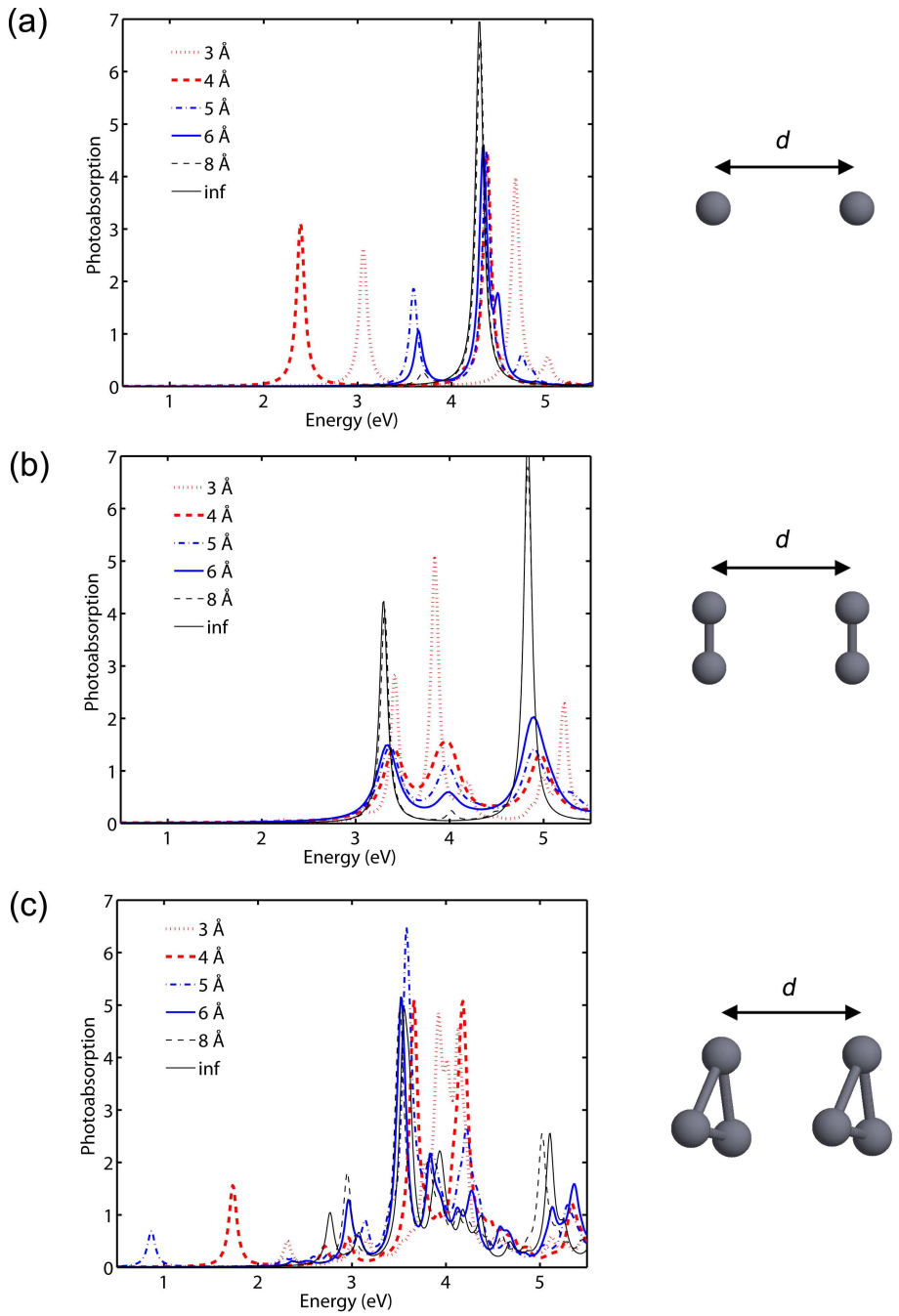

Figure 5.6: Calculated optical absorption spectra of two silver (a) monomers, (b) dimers, and (c) trimers with varying distance d. The structures are illustrated on the right.

Chapter 6

Conclusions

In this Thesis, the optical properties of different nanostructures are investigated using the time-dependent density-functional theory (TDDFT). The studied materials include carbon fullerenes of different sizes and with different substitutional silicon doping, boron nitride fullerenes, silicon nanocrystals (hydrogen passivated and embedded in silica), silver nanoclusters and their hybrid structures with the PMAA polymer.

The OCTOPUS program is our main tool used in all the TDDFT calculations of this work. The OCTOPUS program is a real-time real-space implementation of TDDFT which contains also frequency-space methods such as the Casida method.

For fullerenes and their derivatives, the main question addressed in this Thesis is whether (minor) structural changes can be detected using absorption spectroscopy. The silicon doping of buckminsterfullerenes resulted in clear spectral changes as reported in Publication I. For small fullerenes, a shift of the main low-energy transition as a function of the size is found and relations between geometries and absorption spectra are observed. Also in the case of boron nitride fullerenes in Publication II, different isomers are distinguishable by the calculated spectra and some of the spectral features can be associated with geometric aspects of the specific structures.

In Publication III, the effect of the environment on the photoabsorption of silicon nanorystals is studied. The well-known size dependence of hydrogen-passivated nanocrystals is observed: the absorption edge shifts to lower energies as the size of the crystal increases. Surprisingly, for Si-nanocrystals embedded in silica, a qualitatively different result is obtained. An almost constant absorption edge at about 3 eV (blue end of the visible range) is observed in the crystal size range of Si_{17}–Si_{47}. This is explained by the localization of some of the electron states near the HOMO-LUMO gap in the vicinity of the Si-SiO_2 interface.

Finally, experimentally observed unexpected luminescence properties of hybrid silver cluster-PMAA polymer systems inspired us to study the effect of chemical environment on the optical properties of silver clusters. Publication IV presents results which confirm that the presence of a polymer might indeed have a huge impact on the absorption characteristics. Low-energy absorption appears in cases where local spin polarization occurs in the silver cluster in hybrid systems. Also the opposite effect, the quenching of low-energy excitations in silver clusters in the presence of the polymer, is recorded in certain hybrid structures with no spin polarization.

In addition, the effect of the interaction between pure cluster pairs at distances above bonding lengths is studied. The electron clouds of the clusters interact remarkably up to the distance of about 6 Å. This interaction can be seen as clear changes in the absorption spectra in comparison with the spectra of separated clusters.

Bibliography

[1] C. Fiolhais, F. Nogueira, and M. Marques, eds., *A Primer in Density Functional Theory* (Springer-Verlag, Berlin Heidelberg, 2003).

[2] P. Hohenberg and W. Kohn, *Inhomogeneous Electron Gas*, Phys. Rev. **136**, B864 (1964).

[3] W. Kohn and L. J. Sham, *Self-Consistent Equations Including Exchange and Correlation Effects*, Phys. Rev. **140**, A1133 (1965).

[4] M. A. L. Marques, C. A. Ullrich, F. Nogueira, A. Rubio, K. Burke, and E. K. U. Gross, eds., *Time-Dependent Density Functional Theory* (Springer-Verlag, Berlin Heidelberg, 2006).

[5] P. Elliott, K. Burke, and F. Furche, *Excited states from time-dependent density functional theory*, Rev. Comput. Chem. **26**, 91 (2008).

[6] E. Runge and E. K. U. Gross, *Density-Functional Theory for Time-Dependent Systems*, Phys. Rev. Lett. **52**, 997 (1984).

[7] D. Marx and J. Hutter, *Ab Initio Molecular Dynamics: Basic Theory and Advanced Methods* (Cambridge University Press, Cambridge, UK, 2009).

[8] M. Di Ventra, ed., *Electrical Transport in Nanoscale Systems* (Cambridge University Press, Cambridge, UK, 2008).

[9] S. Kurth, G. Stefanucci, A. C.-O., A. Rubio, and E. K. U. Gross, *Time-dependent quantum transport: A practical scheme using density functional theory*, Phys. Rev. B **72**, 035308 (2005).

[10] J. Z. Zhang, *Optical properties and spectroscopy of nanomaterials* (World Scientific Publishing, Singapore, 2009).

[11] X. Xing, B. Yoon, U. Landman, and J. H. Parks, *Structural evolution of Au nanoclusters: From planar to cage to tubular motifs*, Phys. Rev. B **74**, 165423 (2006).

[12] W. Huang, R. Pal, L.-M. Wang, X. C. Zeng, and L.-S. Wang, *Isomer identification and resolution in small gold clusters*, J. Chem. Phys. **132**, 054305 (2010).

[13] E. K. Parks, L. Zhu, J. Ho, and S. J. Riley, *The structure of small nickel clusters II Ni_{16}–Ni_{28}*, J. Chem. Phys. **102**, 7377 (1995).

[14] S. Goedecker, W. Hellmann, and T. Lenosky, *Global Minimum Determination of the Born-Openheimer Surface within Density Functional Theory*, Phys. Rev. Lett. **95**, 055501 (2005).

[15] M. Levy, *Electron densities in search of Hamiltonians*, Phys. Rev. A **26**, 1200 (1982).

[16] J. C. Slater, *A Simplification of the Hartree-Fock Method*, Phys. Rev. **81**, 385 (1951).

[17] J. P. Perdew and A. Zunger, *Self-interaction correction to density-functional approximations for many-electron systems*, Phys. Rev. B **23**, 5048 (1981).

[18] L. D. C. and M. J. Mehl, *Beyond the local-density approximation in calculations of ground-state electronic properties*, Phys. Rev. B **28**, 1809 (1983).

[19] A. D. Becke, *Density-functional exchange-energy approximation with correct asymptotic behavior*, Phys. Rev. A **38**, 3098 (1988).

[20] J. P. Perdew, K. Burke, and M. Ernzerhof, *Generalized Gradient Approximation Made Simple*, Phys. Rev. Lett. **77**, 3865 (1996).

[21] J. P. Perdew, S. Kurth, A. Zupan, and P. Blaha, *Accurate Density Functional with Correct Formal Properties: A Step Beyond the Generalized Gradient Approximation*, Phys. Rev. Lett. **82**, 2544 (1999).

[22] C. Lee, W. Yang, and R. G. Parr, *Development of the Colle-Salvetti correlation-energy formula into a functional of the electron density*, Phys. Rev. B **37**, 785 (1988).

[23] P. J. Stephens, F. J. Devlin, C. F. Chabalowski, and M. J. Frisch, Ab Initio *Calculation of Vibrational Absorption and Circular Dichroism Spectra Using Density Functional Force Fields*, J. Phys. Chem. **98**, 11623 (1994).

[24] A. D. Becke, *A new mixing of Hartree-Fock and local density-functional theories*, J. Chem. Phys. **98**, 1372 (1993).

[25] A. D. Becke, *Density-functional thermochemistry. III. The role of exact exchange*, J. Chem. Phys. **98**, 5648 (1993).

[26] S. Kümmel and L. Kronik, *Orbital-dependent density functionals: Theory and applications*, Rev. Mod. Phys. **80**, 3 (2008).

[27] O. Gunnarsson and B. I. Lundqvist, *Exchange and correlation in atoms, molecules, and solids by the spin-density-functional formalism*, Phys. Rev. B **13**, 4274 (1976).

[28] N. I. Gidopoulos, P. G. Papaconstantinou, and E. K. U. Gross, *Spurious Interactions, and Their Correction, in the Ensemble-Kohn-Sham Scheme for Excited States*, Phys. Rev. Lett. **88**, 033003 (2002).

[29] V. R. Saunders and J. H. van Lenthe, *The direct CI method*, Mol. Phys. **48**, 923 (1983).

[30] R. J. Buenker, S. D. Peyerimhoff, and W. Butscher, *Applicability of the multi-reference double-excitation CI (MRD-CI) method to the calculation of electronic wavefunctions and comparison with related techniques*, Mol. Phys. **35**, 771 (1978).

[31] D. M. Ceperley and B. Bernu, *The calculation of excited state properties with quantum Monte Carlo*, J. Chem. Phys. **89**, 6316 (1988).

[32] B. Bernu, D. M. Ceperley, and J. Lester, W. A., *The calculation of excited states with quantum Monte Carlo. II. Vibrational excited states*, J. Chem. Phys. **93**, 552 (1990).

[33] C. Møller and M. S. Plesset, *Note on an Approximation Treatment for Many-Electron Systems*, Phys. Rev. **46**, 618 (1934).

[34] L. J. Sham and T. M. Rice, *Many-Particle Derivation of the Effective-Mass Equation for the Wannier Exciton*, Phys. Rev. **144**, 708 (1966).

[35] L. Hedin, *New Method for Calculating the One-Particle Green's Function with Application to the Electron-Gas Problem*, Phys. Rev. **139**, A796 (1965).

[36] G. Onida, L. Reining, and A. Rubio, *Electronic excitations: density-functional versus many-body Green's-function approaches*, Rev. Mod. Phys. **74**, 601 (2002).

[37] S. Botti, A. Schindlmayr, R. Del Sole, and L. Reining, *Time-dependent density-functional theory for extended systems*, Rep. Prog. Phys. **70**, 357 (2007).

[38] N. T. Maitra, *Initial-State Dependence and Memory*, Lect. Notes Phys. **706**, 61 (2006).

[39] R. van Leeuwen, *Causality and Symmetry in Time-Dependent Density-Functional Theory*, Phys. Rev. Lett. **80**, 1280 (1998).

[40] K. Yabana and G. F. Bertsch, *Time-dependent local-density approximation in real time*, Phys. Rev. B **54**, 4484 (1996).

[41] M. Petersilka, E. K. U. Gross, and K. Burke, *Excitation energies from time-dependent density functional theory using exact and approximate potentials*, Int. J. Quantum Chem. **80**, 534 (2000).

[42] J. Olsen and P. Jørgensen, *Linear and nonlinear response functions for an exact state and for an MCSCF state*, J. Chem. Phys. **82**, 3235 (1985).

[43] M. E. Casida, in *Recent Developments and and Application of Modern Density Functional Theory*, edited by J. M. Seminario (Elsevier, Amsterdam, 1996), pp. 391–439.

[44] M. Petersilka, U. J. Gossmann, and E. K. U. Gross, *Excitation Energies form Time-Dependent Density-Functional Theory*, Phys. Rev. Lett. **76**, 1212 (1996).

[45] M. A. L. Marques, A. Castro, G. F. Bertsch, and A. Rubio, *Octopus: a first-principles tool for excited-ion dynamics*, Comput. Phys. Commun. **151**, 60 (2003).

[46] A. Castro, H. Appel, M. Oliveira, C. A. Rozzi, X. Andrade, F. Lorenzen, M. A. L. Marques, E. K. U. Gross, and A. Rubio, *Octopus: a tool for the application of time-dependent density functional theory*, Phys. Status Solidi B **243**, 2465 (2006), `http://www.tddft.org/programs/octopus/`.

[47] J. J. Mortensen, L. B. Hansen, and K. W. Jacobsen, *Real-space grid implementation of the projector augmented wave method*, Phys. Rev. B **71**, 035109 (2005).

[48] M. Walter, H. Häkkinen, L. Lehtovaara, M. Puska, J. Enkovaara, Rostgaard, and J. J. C. Mortensen, *Time-dependent density-functional theory in the projector augmented-wave method*, J. Chem. Phys. **128**, 244101 (2008).

[49] A. Castro, M. A. L. Marques, and A. Rubio, *Propagators for the time-dependent Kohn-Sham equations*, J. Chem. Phys. **121**, 3425 (2004).

[50] N. Troullier and J. L. Martins, *Efficient pseudopotentials for plane-wave calculations*, Phys. Rev. B **43**, 1993 (1991).

[51] P. Blöchl, *Projector augmented-wave method*, Phys. Rev. B **50**, 17953 (1995).

[52] H. W. Kroto, J. R. Heath, S. C. O'Brien, R. F. Curl, and R. E. Smalley, *C_{60}: Buckminsterfullerene*, Nature **318**, 162 (1985).

[53] S. Iijima, *Helical microtubules of graphitic carbon*, Nature **354**, 56 (1991).

[54] Y. Gogotsi, ed., *Carbon Nanomaterials* (Taylor and Francis Group, Boca Raton, FL, USA, 2006).

[55] K. S. Novoselov, A. K. Geim, S. V. Morozov, D. Jiang, Y. Zhang, S. V. Dubonos, I. V. Grigorieva, and A. A. Firsov, *Electric Field Effect in Atomically Thin Carbon Films*, Science **306**, 666 (2004).

[56] A. G. Nasibulin, P. V. Pikhitsa, H. Jiang, D. P. Brown, A. V. Krasheninnikov, A. S. Anisimov, P. Queipo, A. Moisala, D. Gonzalez, G. Lientschnig, et al., *A novel hybrid carbon material*, Nature Nanotech. **2**, 156 (2007).

[57] F. Langa and J.-F. Nierengarten, eds., *Fullerenes: Principles and Applications* (The Royal Society of Chemistry, Cambridge, UK, 2007).

[58] P. R. C. Kent, M. D. Towler, R. J. Needs, and G. Rajagopal, *Carbon clusters near the crossover to fullerene stability*, Phys. Rev. B **62**, 15394 (2000).

[59] C. C. Piskoti, J. Yarger, and A. Zeitl, *C_{36}, a new carbon solid*, Nature **393**, 771 (1998).

[60] X. Lu and Z. Chen, *Curved Pi-Conjugation, Aromaticity, and the Related Chemistry of Small Fullerenes ($< C_{60}$) and Single-Walled Carbon Nanotubes*, Chem. Rev. **105**, 3643 (2005).

[61] E. Małolepsza, H. A. Witek, and S. Irle, *Comparison of Geometric, Electronic, and Vibrational Properties for Isomers of Small Fullerenes C_{20}–C_{36}*, J. Phys. Chem. A **111**, 6649 (2007).

[62] H. Prinzbach, A. Weiler, P. Landenberger, F. Wahl, J. Wörth, L. T. Scott, M. Gelmont, D. Olevano, and B. v. Issendorff, *Gas-phase production and photoelectron spectroscopy of the smallest fullerene, C_{20}*, Nature **407**, 60 (2000).

[63] A. Castro, M. A. L. Marques, J. A. Alonso, G. F. Bertsch, K. Yabana, and A. Rubio, *Can optical spectroscopy directly elucidate the ground state of C_{20}*, J. Chem. Phys. **116**, 1930 (2002).

[64] R.-H. Xie, G. W. Bryan, C. F. Cheung, V. H. J. Smith, and J. Zhao, *Optical excitation and absorption spectra of $C_{50}Cl_{10}$*, J. Chem. Phys. **121**, 2849 (2004).

[65] S.-Y. Xie, F. Gao, X. Lu, R.-B. Huang, C.-R. Wang, X. Zhang, M.-L. Liu, S.-L. Deng, and L.-S. Zheng, *Capturing the Labile Fullerene[50] as $C_{50}Cl_{10}$*, Science **304**, 699 (2004).

[66] M. L. Tiago, P. R. C. Kent, R. Q. Kent, and F. A. Reboredo, *Neutral and charged excitations in carbon fullerenes from first-principles many-body theories*, J. Chem. Phys. **129**, 084311 (2008).

[67] J. Wang, Y. Liu, and Y.-C. Li, *Magnetic silicon fullerene*, arxiv:0908.1494v1 (2009).

[68] C. Pellarin, M. Ray, J. Lermé, J. L. Vialle, M. Broyer, X. Blase, P. Kéghélian, P. Mélinon, and A. Perez, *Photolysis experiments on SiC mixed clusters: From silicon carbide clusters to silicon-doped fullerenes*, J. Chem. Phys. **110**, 6927 (1999).

[69] M. Matsubara and C. Massobrio, *Stability of charged Si-doped heterofullerenes: A first-principles molecular dynamics study*, Phys. Rev. B **79**, 155411 (2009).

[70] M. Matsubara, J. Kortus, J.-C. Parlebas, and C. Massobrio, *Dynamical Identification of a Threshold Instability in Si-Doped Heterofullerenes*, Phys. Rev. Lett. **96**, 155502 (2006).

[71] C.-C. Fu, M. Weissman, M. Machado, and P. Ordejón, *Ab initio study of silicon-multisubstituted neutral and charged fullerenes*, Phys. Rev. B **63**, 085411 (2001).

[72] M. Matsubara and C. Massobrio, *Bonding behavior and thermal stability of $C_{54}Si_6$: A first-principles molecular dynamics study*, J. Chem. Phys. **122**, 084304 (2005).

[73] N. G. Chopra, R. J. Luyken, K. Cherrey, V. H. Crespi, M. L. Cohen, S. G. Louie, and A. Zettl, *Boron Nitride Nanotubes*, Science **269**, 966 (1995).

[74] L. Boulanger, B. Andriot, M. Cauchetier, and F. Willaime, *Concentric shelled and plate-like graphitic boron nitride nanoparticles produced by CO_2 laser pyrolysis*, Chem. Phys. Lett. **234**, 227 (1995).

[75] O. Stéphan, Y. Bando, A. Loiseau, F. Willamie, N. Shramchenko, T. Tamiya, and T. Sato, *Formation of small single-layer and nested BN cages under electron irradiation of nanotubes and bulk material*, Appl. Phys. A: Mater. Sci. Process. **67**, 107 (1998).

[76] D. Goldberg, Y. Bando, O. Stéphan, and K. Kurashima, *Octahedral boron nitride fullerenes formed by electron beam irradiation*, Appl. Phys. Lett. **73**, 2441 (1998).

[77] S. A. Shevlin, Z. X. Guo, H. J. J. van Dam, P. Sherwood, C. R. A. Catlow, A. A. Sokol, and S. M. Woodley, *Structure, optical properties and defects in nitride (III–V) nanoscale cage clusters*, Phys. Chem. Chem. Phys. **10**, 1944 (2008).

[78] W. H. Moon, S. S. Son, and H. J. Hwang, *Theoretical study on structure of boron nitride fullerenes*, Applied Surface Science **253**, 7078 (2007).

[79] R. J. C. Batista, M. S. C. Mazzoni, and H. Chacham, *Boron nitride fullerene $B_{36}N_{36}$ doped with transition metal atoms: First principles calculations*, Phys. Rev. B **75**, 035417 (2007).

[80] R. R. Zope and B. I. Dunlap, *Electronic structure of fullerenelike cages and finite nanotubes of aluminum nitride*, Phys. Rev. B **72**, 045439 (2005).

[81] N. Gonzalez Szwacki, A. Sadrzadeh, and B. I. Yakobson, *B_{80} Fullerene: An Ab Initio Prediction of Geometry, Stability, and Electronic Structure*, Phys. Rev. Lett. **98**, 166804 (2007).

[82] S. Botti, A. Castro, N. Lathiotakis, X. Andrade, and M. A. L. Marques, *Optical and magnetic properties of boron fullerenes*, Phys. Chem. Chem. Phys. **11**, 4523 (2009).

[83] M. Bar-Sadan, I. Kaplan-Ashiri, and R. Tenne, *Inorganic fullerenes and nanotubes: Wealth of materials and morphologies*, Eur. Phys. J. Special Topics **149**, 71 (2007).

[84] L. Khriachtchev, ed., *Silicon Nanophotonics* (World Scientific Publishing, Singapore, 2008).

[85] N. Daldosso and L. Pavesi, *Nanosilicon photonics*, Laser & Photon. Rev. pp. 1–27 (2009).

[86] N. Koshida, ed., *Device Applications of Silicon Nanocrystals and Nanostructures* (Springer, New York, 2009).

[87] V. Kumar, ed., *Nanosilicon* (Elsevier, Oxford, 2007).

[88] L. T. Canham, *Silicon quantum wire array fabrication by electrochemical and chemical dissolution of wafers*, Appl. Phys. Lett. **57**, 1046 (1990).

[89] L. Pavesi, L. Dal Negro, C. Mazzoleni, G. Franzò, and F. Priolo, *Optical gain in silicon nanocrystals*, Nature **408**, 440 (2000).

[90] L. Khriachtchev, T. Nikitin, R. Velagapudi, J. Lahtinen, and S. Novikov, *Light-emission mechanism of thermally annealed silicon-rich silicon oxide revisited: What is the role of silicon nanocrystals?*, Appl. Phys. Lett. **94**, 043115 (2009).

[91] S. Hernández, P. Pellegrino, A. Martínez, Y. Lebour, B. Garrido, R. Spano, M. Cazzanelli, N. Daldosso, L. Pavesi, E. Jordana, et al., *Linear and nonlinear optical properties of Si nanocrystals in SiO_2 deposited by plasma-enhanced chemical-vapor deposition*, J. Appl. Phys. **103**, 064309 (2008).

[92] G. Allan, C. Delerue, and M. Lannoo, *Nature of Luminescent Surface States of Semiconductor Nanocrystallites*, Phys. Rev. Lett. **76**, 2961 (1996).

[93] O. Lehtonen and D. Sundholm, *Bright luminescence from silane substituted and bridged silicon nanoclusters*, Phys. Chem. Chem. Phys. **8**, 4228 (2006).

[94] L. E. Ramos, J. Paier, G. Kresse, and F. Bechstedt, *Optical spectra of Si nanocrystallites: Bethe-Salpeter approach versus time-dependent density-functional theory*, Phys. Rev. B **78**, 195423 (2008).

[95] R. J. Eyre, J. P. Goss, and P. R. Briddon, *Effect of progressive oxidation on the optical properties of small silicon quantum dots: A computational study*, Phys. Rev. B **77**, 245407 (2008).

[96] M. Luppi and S. Ossicini, *Ab initio study on oxidized silicon clusters and silicon nanocrystals embedded in SiO_2: Beyond the quantum confinement effect*, Phys. Rev. B **71**, 035340 (2005).

[97] M. Gatti and G. Onida, *Effects of local fields in time-dependent density functional theory shown in oxidized silicon clusters*, Phys. Rev. B **72**, 045442 (2005).

[98] R. J. Eyre, J. P. Goss, and P. R. Briddon, *Density functional study of oxygen migration processes for silicon quantum dots*, Phys. Rev. B **76**, 245325 (2007).

[99] L. E. Ramos, J. Furthmüller, and F. Bechstedt, *Effect of backbond oxidation on silicon nanocrystallites*, Phys. Rev. B **70**, 033311 (2004).

[100] L. E. Ramos, J. Furthmüller, and F. Bechstedt, *Influence of oxygen on optical properties of Si nanocrystallites*, Appl. Phys. Lett. **87**, 143113 (2005).

[101] L. E. Ramos, J. Furthmüller, and F. Bechstedt, *Reduced influence of defects on oxidized Si nanocrystallites*, Phys. Rev. B **71**, 035328 (2005).

[102] R. Guerra, I. Marri, R. Magri, L. Martin-Samos, O. Pulci, E. Degoli, and S. Ossicini, *Silicon nanocrystallites in a SiO_2 matrix: Role of disorder and size*, Phys. Rev. B **79**, 155320 (2009).

[103] F. Djurabekova and K. Nordlund, *Atomistic simulation of the interface structure of Si nanocrystals embedded in amorphous silica*, Phys. Rev. B **77**, 115325 (2008).

[104] S. Fedrigo, W. Harbich, and J. Buttet, *Collective dipole oscillations in small silver clusters embedded in rare-gas matrices*, Phys. Rev. B **47**, 10706 (1993).

[105] J. P. Wilcoxon and B. L. Abrams, *Synthesis, structure and porperties of metal nanoclusters*, Chem. Soc. Rev. **35**, 1162 (2006).

[106] K. Yabana and G. F. Bertsch, *Optical response of small silver clusters*, Phys. Rev. A **60**, 3809 (1999).

[107] J. C. Idrobo, S. Öğüt, and J. Jellinek, *Size dependence of the static polarizabilities and absorption spectra of Ag_n ($n = 2-8$) clusters*, Phys. Rev. B **72**, 085445 (2005).

[108] M. L. Tiago, J. C. Idrobo, S. Öğüt, J. Jellinek, and J. R. Chelikowsky, *Electronic and optical excitations in Ag_n clusters ($n = 1 - 38$): Comparison of density-functional and many-body theories*, Phys. Rev. B **79**, 155419 (2009).

[109] M. Harb, F. Rabilloud, and D. Simon, *Optical absorption of silver clusters: A study of the effective potential core size*, Chem. Phys. Lett. **476**, 186 (2009).

[110] I. Díez, M. Pusa, S. Kulmala, H. Jiang, A. Walther, A. S. Goldmann, A. H. E. Müller, O. Ikkala, and R. H. A. Ras, *Color Tunability and Electrochemiluminescence of Silver Nanoclusters*, Angew. Chem. Int. Ed. **48**, 2122 (2009).

[111] L. Shang and S. Dong, *Facile preparation of water-soluble fluorescent silver nanoclusters using a polyelectrolyte template*, Chem. Comm. **2008**, 1088 (2008).

[112] R. Konradi and J. Rühe, *Interaction of Poly(methacrylic acid) Brushes with Metal Ions: Swelling Properties*, Macromolecules **38**, 4345 (2005).

[113] L. Peyser-Capadona, J. Zheng, J. I. González, T.-H. Lee, S. A. Patel, and R. M. Dickson, *Nanoparticle-Free Single Molecule Anti-Stokes Raman Spectroscopy*, Phys. Rev. Lett. **94**, 058301 (2005).

[114] R. Mitrić, J. Petersen, A. Kulesza, and V. Bonačić-Koutecký, *Photoabsorption and photofragmentation of isolated cationic silver cluster-tryptophan systems*, J. Chem. Phys. **127**, 134301 (2007).

[115] A. Kulesza, R. Mitrić, and V. Bonačić-Koutecký, *Silver cluster induced absorption enhancement and conformation control of peptides*, Eur. Phys. J. D **52**, 203 (2009).

[116] G. J. H. Giesbertz, E. J. Baerdens, and O. V. Gritsenko, *Charge Transfer, Double and Bond-Breaking Excitations with Time-Dependent Density Matrix Functional Theory*, Phys. Rev. Lett. **101**, 033004 (2008).